AIAA JOURNAL
Vol. 37, No. 10, October 1999

Aspects of Flow Structure During a Cylinder Wake-Induced Laminar/Turbulent Transition

N. K. Kyriakides,* E. G. Kastrinakis,† S. G. Nychas,‡ and A. Goulas§
Aristotle University of Thessaloniki, 540 06 Thessaloniki, Greece

The process of a strong wake-induced laminar/turbulent transition on a flat-plate boundary layer was investigated from the point of view of the occurring coherent structures. The wake was generated by a horizontal cylinder positioned in the freestream and upstream of the flat plate's leading edge. An X-type hot-wire probe measured the streamwise and normal-to-the-wall velocity components, whereas a gradient hot-wire probe, located in the cylinder's wake and at the same streamwise position as the X-type hot-wire probe, detected the passage of the von Kármán vortices. From the simultaneously acquired velocity and gradient signals, the intermittency factor distribution and cross-correlation functions, combined with a quadrant-splitting analysis, were computed. Furthermore, an ensemble-average technique was applied to the signals. The analysis of the signals revealed that during the transition a secondary vortical structure occurs near the wall. Turbulent kinetic energy transfer to and from the wall during the transition was evaluated.

Nomenclature

d	= cylinder diameter
f_{sr}	= Strouhal frequency of the von Kármán vortex street
H	= shape factor of the boundary layer
$Q1$	= interactions outward
$Q2$	= ejections
$Q3$	= interactions wallward
$Q4$	= sweeps
$R_{xy,Qi}$	= cross-correlation function
Sr	= Strouhal number, $=f_{sr}\,\mathrm{d}/U_0$
T_{sr}	= Strouhal period
Tu	= freestream turbulence intensity
t	= time
t^+	= dimensionless time, $=tu_\tau^2/\nu$
t_{sr}^+	= dimensionless Strouhal period
t_Λ	= timescale of the Λ shape
t_Λ^+	= dimensionless timescale of the Λ shape
U	= instantaneous streamwise velocity
$\bar{U}$	= time-averaged streamwise velocity
U_c	= local convection velocity
U_o	= freestream velocity
u	= streamwise velocity fluctuation
uv	= instantaneous Reynolds stress
$\overline{uv}$	= time-averaged Reynolds stress
uv_{mean}	= ensemble average of the uv signal
uv_{Qi}	= instantaneous Reynolds stress of the Qi quadrant
$\overline{uv_{Qi}}$	= time-averaged Reynolds stress of the Qi quadrant
uv_{rms}	= ensemble rms value of the uv signal
u_τ	= friction velocity
V	= instantaneous normal-to-the-wall velocity
$\bar{V}$	= time-averaged normal-to-the-wall velocity component
v	= instantaneous fluctuation of the normal-to-the-wall velocity
w	= instantaneous fluctuation of the lateral velocity
x	= streamwise position with respect to the plate's leading edge
x_c	= streamwise position of the cylinder
x_{onset}	= streamwise location of the transition onset
x^+	= nondimensional streamwise distance, $=xu_\tau/\nu$
y	= distance normal to the plate surface
y_c	= normal-to-the-wall position of the cylinder
y_Λ	= y extent of the Λ shape
y^+	= nondimensional distance from the wall, $=yu_\tau/\nu$
y_Λ^+	= dimensionless y extent of the Λ shape
γ	= intermittency factor
δ_1	= displacement thickness
δ_2	= momentum thickness
λ	= streamwise region where γ increases from $\gamma = 0.25$ to 0.75
ν	= kinematic viscosity of air
ξ	= threshold constant
τ	= time delay
Ψ	= stream function
ω_z	= spanwise vorticity

Received 16 July 1998; revision received 22 February 1999; accepted for publication 22 February 1999.

*Postdoctoral Researcher, Department of Chemical Engineering.
†Assistant Professor, Department of Chemical Engineering.
‡Professor, Department of Chemical Engineering.
§Professor, Department of Mechanical Engineering.

I. Introduction

In aeronautics, process engineering, turbomachinery, and other disciplines in engineering, laminar/turbulent transition on a flat solid boundary can be caused through the interaction between vortices occurring outside the boundary layer (e.g., wake vortices) and the boundary-layer flow itself. A transition caused by the vortices of a wake is referred to as a wake-induced laminar/turbulent transition. A step toward the understanding of wake-induced laminar/turbulent transition is the identification and dynamics of the coherent structures that occur during this process. The existence of the wake vortices causes disturbances in the boundary layer of the flat plate in addition to the disturbances in the freestream. Fundamental studies of simple vortex/laminar boundary-layer interactions provide new insight into the physics of the boundary-layer turbulence energy production. Doligalski and Walker[1] investigated analytically the response of a flat-plate boundary layer to the motion of a convected single vortex. They suggested that a strong inviscid/viscous interaction took place in the form of an eruption of the boundary-layer flow. The development of an instantaneous adverse pressure gradient on the wall could create the conditions for the boundary-layer transition. Walker[2] calculated the streamwise pressure gradient near the wall caused by a moving vortex in the region close to the turbulent boundary layer of the flat plate. He noted that a convected vortex above the wall layer, which was predominantly of the hairpin type, provided a moving zone of adverse pressure gradient. When the vortex was strong enough and/or close enough to the wall for a sufficient period of time, an eruption was induced near the wall. On the other hand, weaker disturbances could provoke an instability in the wall layer. In both cases, a local breakdown of the relatively well-ordered near-wall flow occurred. Ersoy and Walker[3] studied analytically a boundary layer disturbed by a pair of longitudinal vortices

of opposite vorticity. In this case a region of flow separation was developed on the wall. Three-dimensional separation phenomena were also observed in the study of Ersoy and Walker.[4] In this case the boundary layer was disturbed by a vortex loop.

Gartshore et al.[5] applied rapid-distortion theory to study how external turbulence affected an adjacent initially turbulence-free region in which a mean velocity gradient existed. They showed that external turbulence first induced irrotational velocity fluctuations, which subsequently interacted with the shear and produced rotational velocity fluctuations and Reynolds stresses. The rapid-distortion theory indicates that these stresses extend into the sheared region over a distance of the order of the integral scale. Experimental measurements confirmed their predictions. Luton et al.[6] simulated numerically the interaction of a laminar boundary layer with a spanwise vortex. They found that the strong vortex they considered induces an eruption and a production of a secondary vortex, which causes the primary vortex to rebound.

In a review of boundary-layer/wake interaction, Squire[7] has indicated that the upstream wake increases the overall turbulence level in the flow and thus brings the transition process forward. On a more fundamental basis, Savill and Zhou[8] made an extensive study at low Reynolds numbers of various types of simple interactions using flow visualization. Wakes formed behind a circular cylinder were examined to obtain an essentially two-dimensional vortex street. They studied what was called slow or weak interactions, in which the wake was initially sufficiently far from the boundary layer and was effectively fully developed, before it started to merge with the boundary layer. In contrast to this type of transition, fast or strong interactions were also studied. In this type of interaction, the initial vortex street was still present when the two shear layers merged.

The purpose of the present work was the identification and study of coherent structures occurring during the boundary-layer transition induced by a von Kármán wake. To this end, techniques of signal analysis were applied, which included computation of cross-correlation functions combined with a quadrant-splitting analysis and an ensemble-average technique.

II. Experimental Facility

The experiments were carried out in a low-speed boundary-layer wind tunnel at a freestream velocity of $U_o = 5$ m/s (see also Refs. 9 and 10). The freestream turbulence intensity $Tu = (\overline{u^2})^{1/2}/U_o$ in the wind tunnel was around 0.004. From the velocity measurements the friction velocity u_τ was determined, and an average value of $u_\tau = 25$ cm/s was taken for the purpose of this presentation. The horizontal test section of the wind tunnel was 0.6×0.6 m in cross section and 2 m in length. The transition process was studied on a 1.24-m-long aluminum flat plate, which spanned the whole test section width of 0.6 m and was positioned at 30 cm above the bottom of the test section while its leading edge was sharp (radius 0.5 mm). Confinement effects of the flow in the transverse direction were negligible. The flat plate was first placed horizontally using an appropriate spirit level, and afterward it was positioned at an incidence angle of -0.5 deg to avoid leading-edge separation. Mean pressure measurements along the plate were conducted on the upper wall, and no adverse pressure gradient was detected. The plate was mounted to an independent supporting system, which was installed outside the tunnel; the system was provided with vibration insulating elements. In this manner vibrations of the wind tunnel walls were not transmitted to the plate as it was nowhere in contact with the tunnel itself.

A cylinder with a diameter of $d = 10$ mm positioned upstream and parallel to the leading edge of the plate was used to generate a two- dimensional wake, which interacted with the flow above the flat plate and the developing boundary layer. The cylinder Reynolds number was 3500, and its wake was turbulent. The horizontal position of the cylinder was examined by a spirit level. A general view of the experimental arrangement is given in Fig. 1. The cylinder was placed at the position $x_c = -10$ mm and $y_c = 25$ mm from the leading edge of the flat plate. Special precautions, as proposed by Van Atta and Gharib,[11] were taken to avoid cylinder vibrations. According to Van Atta and Gharib, a vibrating cylinder develops a vortex street with unpredictable differences in the Strouhal frequency and

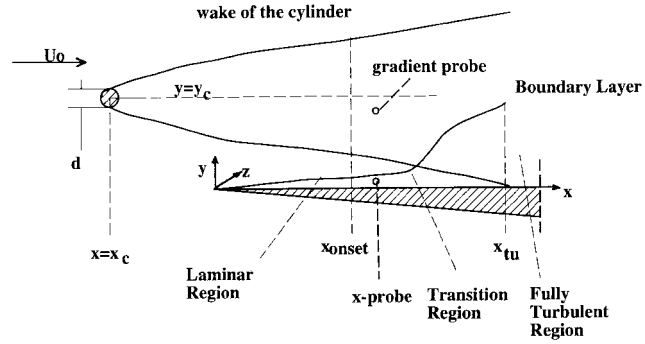

Fig. 1 Sketch of the experimental arrangement.

a wake that is unsteady. In the present experiments the formation of a steady-state wake was necessary; this was ensured by examining the velocity energy spectra, which had a single peak at the Strouhal frequency corresponding to the freestream velocity.

An X-type hot-wire probe (Dantec 55P53) was used for the simultaneous measurement of the streamwise velocity component U and the velocity component normal to the wall V at various (x, y) positions in the boundary layer. To be able to approach the plate surface at small distances, the prongs of the hot-wire sensors were inclined at an angle of 90 deg with respect to the main axis of the probe. A gradient hot-wire probe (Dantec 55P71), consisting of two parallel wires, was located in the wake of the cylinder for several y distances $(y < y_c)$ from the wall, measured the local instantaneous gradient $\partial U/\partial y$ of the streamwise velocity component. The instantaneous gradient was used as a qualitative detector of the von Kármán structure. For both hot-wire probes used, the hot-wire sensors had a diameter of 5 μm and a length of 1.25 mm, whereas the sensor support had a diameter of 2.3 mm and a length of 33 mm. As shown in Fig. 1, the two probes were positioned at the same x distance by supporting the corresponding probe holders on the same traversing base. Two manually controlled traversing mechanisms, with a total displacement of 20 cm in the streamwise direction and 20 cm in the normal direction and with an accuracy of 0.01 mm, were used for the x and y traversing of the hot-wire probes, respectively. A supplementary traversing mechanism with an accuracy of 0.5 mm was used only for longer x displacements of the whole system. The calibrations of the two probes were carried out in the test section of the wind tunnel; during the calibration the cylinder was removed. The instantaneous signals from the X- and gradient probes were acquired simultaneously for the various x positions along the plate. Four constant-temperature anemometers (Dantec 55M01) were used. The hot-wire signals passed through a DC-offset controller, a gain amplifier, and a low-pass filter before being digitized by a 16-bit resolution A/D converter. The duration of the data acquisition at each position was 12.5 s, and the corresponding sampling frequency was 4 kHz. This duration proved to be adequate for the proper statistical analysis of the signals.

The probe position closest to the wall was measured by positioning underneath the probe tip a standard microscope glass plate of 0.2-mm thickness. All other distances from the wall were referenced with respect to that position. Therefore the accuracy of the absolute y position was of the order of 0.1 mm. Alternatively, the relative y positions were accurate to within ± 0.01 mm (accuracy of the traversing mechanism).

Errors in the measurements because of the calibration procedure were taken into account. Drifting of the X-type hot-wire probe caused by temperature variation or other factors was monitored by calibrating before and after a specific measurement. In this manner this error was kept to levels of about 1% for each velocity component. On the other hand, errors caused by the three-dimensional flow were considered. More specifically, the error caused by the lateral velocity component w was estimated in a way similar to the one used by Kastrinakis and Eckelmann.[12] Supposing a w component of around 5% of local streamwise velocity, this error was estimated to be around 0.5% of the local mean velocity. Another source of

error examined was the one caused by heat losses because of the proximity of hot-wire sensors to the wall of the aluminum plate. This kind of error has been examined by, among others, Wills[13] and Oka and Kostic.[14] For the closest distance of 0.7 mm measured here, according to the references cited, the estimated error was negligible.

Measurements with all standard X-type hot-wire probes are influenced by the velocity gradients, and the error introduced is larger close to solid walls. For the present measurements error estimates for the closest-to-the-wall distance of 0.7 mm have been carried out based on the influence of the $\partial U/\partial y$ gradient and the analysis presented by Eckelmann et al.[15] and Vukoslavcevic and Wallace.[16] Concerning the instantaneous streamwise velocity component, the maximum relative error based on the $\bar{U}$ was estimated to be up to 10%. Regarding now the local mean $\bar{U}$, this was independently measured with a single boundary-layer probe (Dantec 55P15), and for the closest-to-the-wall distance, these measurements differed from the corresponding X-probe data to around 1%. Concerning the instantaneous normal-to-the-wall velocity component v, the corresponding error based on the maximum instantaneous v was estimated to be up to 30%. This error, however, rapidly decreases with increasing wall distance, as shown in the references just cited.

The gradient probe was used as an approximate ω_z-transverse vorticity detector to be able to identify the passage of vortical structures of the upper and lower branches of the von Kármán vortex street. For this purpose the gradient probe used was adequate. The approximation regarding the vorticity comes also from the fact that the $\partial v/\partial x$ part of the transverse vorticity was not taken into account in these measurements because the v component was not measured by the gradient probe. Related to the phenomena presented here, what is important is the detection of the sequence of the vortices and not necessarily the absolute value of the transverse vorticity.

III. Results

Before the measurements on the process of the wake-induced transition were started, the boundary-layer characteristics without the presence of the cylinder and the cylinder wake characteristics as well were separately studied at the freestream velocity of 5 m/s. In the case of the undisturbed boundary layer, detailed investigations showed that it remained laminar at least up to a streamwise distance of 1000 mm from the sharp leading edge of the plate. The measured boundary-layer velocity profiles were in agreement with the Blasius laminar velocity profile (see also Ref. 9). The maximum turbulence intensity levels within the boundary layer for all x positions between $x = 0$ and 1000 mm varied between 1 and 5% based on the local velocity. The shape factor $H = \delta_1/\delta_2$ (δ_1 is the displacement thickness and δ_2 the momentum thickness of the boundary layer) was always equal to 2.6, indicating that the boundary layer was still laminar.

Measurements were also carried out in the undisturbed wake of the cylinder. To this end, the cylinder was placed far away from the plate. Within the cylinder wake and for several x/d and y/d positions, the two velocity components U and V were measured using an X-hot-wire probe. The measured mean velocity profiles were in agreement with the velocity profiles of a two-dimensional wake behind a cylinder, as given by Schlichting.[17] The characteristic shedding frequency of the wake could be clearly detected up to a distance of $x/d = 80-100$ downstream of the wake origin, which is in agreement with the results of Cimbala et al.[18]; farther downstream the wake decayed. The most probable Strouhal frequency f_{sr} was equal to 95 Hz. This corresponds to a Strouhal number Sr of 0.19.

A. Intermittency Factor

A velocity signal measured in the transition region is composed of both laminar and turbulent parts. The intermittency factor γ is defined as the percentage of time corresponding to turbulent flow. The determination of the turbulent and nonturbulent portions of the transition region and their subsequent separation depends on the technique that is applied to this end. Several difficulties arise in using velocity fluctuations for the determination of the intermittency factor. Velocity fluctuations may be caused by amplified oscillations, as these appear in the present experiments. In their study concerning the determination of the intermittency factor, Keller and Wang[19] suggested that the best criterion is the one based on the square of the instantaneous Reynolds stress, namely the quantity $(uv)^2(t)$. This criterion, which was initially applied by Antonia,[20] proved to be the most efficient.[21]

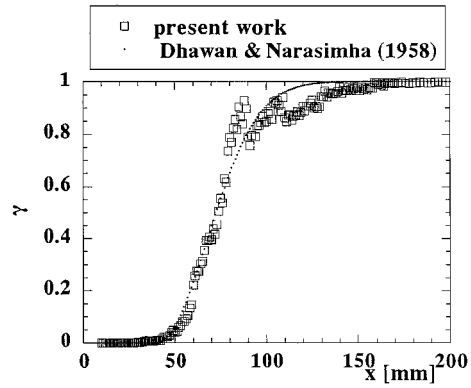

Fig. 2 Intermittency factor as a function of the streamwise distance for $y = 0.7$ mm.

In the present work the $(uv)^2(t)$ signals were used for the determination of the intermittency factor. The quantity $(uv)^2(t)$ in the laminar region was very low. The local mean value of $(uv)^2(t)$ in the laminar region was set as a threshold to specify the turbulent parts of the signal. Downstream of the transition onset, turbulent parts appeared with high uv values. Their durations varied as a function of x. The identification of those signal parts of high energy activity was the basis for the determination of the intermittency factor. Furthermore, the same criterion was used for the estimation of the timescales of turbulent parts in the transition region. Figure 2 shows the distribution of the intermittency factor γ based on the $(uv)^2(t)$ signals as a function of the streamwise distance x for the y distance of 0.7 mm. The distribution of γ indicates several differences compared with the universal one of Dhawan and Narasimha[22] for the transition region. The universal distribution of γ as a function of the streamwise distance x was given by the equation

$$\gamma = 1 - \exp[-0.412(x - x_{\text{onset}})/\lambda] \tag{1}$$

In the present work the intermittency factor attains values greater than zero for streamwise distances larger than the ones corresponding to the transition onset ($x = 33$ mm or $x^+ = 578$). At the streamwise distance $x = 70$ mm ($x^+ = 1225$) a significant difference in the intermittency factor is observed between the experimentally specified γ values and those predicted by Eq. (1). The distribution of the experimentally specified γ shows local minima and maxima for the streamwise positions between $x = 70$ and 120 mm. There are strong indications that this behavior of the γ distribution along the transition region can be attributed to the occurrence and development of certain coherent structures in the transition region. A detailed presentation of these structural aspects will be provided in the discussion section.

B. Cross-Correlation and Quadrant-Splitting Analysis

A cross-correlation analysis of the Reynolds stress signal $uv(t)$ and the gradient signal $(\partial U/\partial y)(t)$ was applied to establish the time relationship between them. The gradient probe was located in the lower part of the cylinder wake, as shown in Fig. 1. Vortices in the wake of the cylinder possess mainly spanwise vorticity ω_z given by the relation

$$\omega_z = \frac{\partial V}{\partial x} - \frac{\partial U}{\partial y} \tag{2}$$

Only the $(\partial U/\partial y)(t)$ signal in the wake was measured with the gradient probe, and it was used as a criterion for the passage of the von Kármán vortices. Taking into account relation (2), a negative velocity gradient $(\partial U/\partial y)$ can be directly associated to a positive vorticity and vice versa.

If one, however, is interested in investigating the flow from the point of view of coherent structures, one should look at the instantaneous fluid motions. More specifically, to associate the passage of a wake vortex (away from the wall) with instantaneously occurring elementary motions near the wall, which are important in the turbulent energy production and transfer, the instantaneous $uv(t)$ signal can be further treated. Toward this direction, Wallace et al.[23] split the instantaneous $uv(t)$ signal into four quadrants, i.e.,

$Q1$ quadrant (interaction outward):

$$u(t) > 0, \quad v(t) > 0, \quad [uv(t) > 0] \tag{3}$$

$Q2$ quadrant (ejection):

$$u(t) < 0, \quad v(t) > 0, \quad [uv(t) < 0] \tag{4}$$

$Q3$ quadrant (interaction wallward):

$$u(t) < 0, \quad v(t) < 0, \quad [uv(t) > 0] \tag{5}$$

$Q4$ quadrant (sweep):

$$u(t) > 0, \quad v(t) < 0, \quad [uv(t) < 0] \tag{6}$$

Their names correspond to visually observed motions (elementary structures or events) in the wall region of fully developed pipe or channel flows. Wallace et al.[23] gave the percentage contributions $\overline{uv_Q}$ of each of the four quadrants (events) to the total Reynolds stress $\overline{uv}$ as a function of the dimensionless distance from the wall y^+ ($y^+ = yu_\tau/\nu$, u_τ is the friction velocity, and ν is the kinematic viscosity of air) in the case of a fully developed turbulent channel flow.

The instantaneous gradient signal, which characterized the von Kármán vortex passage, was correlated with the Reynolds stress signal, which characterized the instantaneously occurring elementary coherent structure. In this way four different cross-correlation functions, each of which corresponds to one of the four quadrants [relations (3–6)], were calculated. They are defined by the relation

$$R_{xy,Qi}(\tau) = \frac{\overline{[-\mathrm{d}U/\mathrm{d}y(t)][uv_{Qi}(t+\tau)]}}{\overline{[(\mathrm{d}U/\mathrm{d}y)^2]}^{\frac{1}{2}}\overline{[(uv_{Qi})^2]}^{\frac{1}{2}}} \tag{7}$$

where i refers to the four quadrants according to relations (3–6). Each cross-correlation function $R_{xy,Qi}(\tau)$ attains its maximum value at a delay time τ. This time τ corresponds to the time difference between the occurrence of the vortex of the von Kármán structure with positive vorticity (at the position of the gradient probe) and the corresponding quadrant Qi (at the position of the X probe).

Following the cross-correlation analysis between the streamwise velocity gradient signal of the wake $\mathrm{d}U/\mathrm{d}y(t)$ and the simultaneous $uv_{Qi}(t)$ signal for every elementary coherent structure of the wall region, the phase time of every quadrant event related to the passage of the von Kármán structure was statistically determined. During the analysis, it was taken into account that the timescale of each elementary quadrant structure was smaller than the Strouhal period. This was experimentally verified by computing the probability distribution of the duration of each elementary structure. The Strouhal period T_{sr} that could be evaluated from the gradient signal was not constant. There was a Strouhal period distribution at every position where measurements were performed. Figure 3 shows probability distributions of T_{sr} for various y positions at the streamwise position $x^+ = 1225$ ($x = 70$ mm); T_{sr} is made dimensionless with the friction velocity u_τ and the kinematic viscosity ν, i.e., $t^+_{sr} = T_{sr}u^2_\tau/\nu$. No detectable y effect concerning the probability distribution of the case of T_{sr} could be detected. From the distributions of T_{sr}, the most probable Strouhal period is 10.5 ms or in nondimensional form $t^+_{sr} = 46$. No detectable y effect concerning this period could be observed.

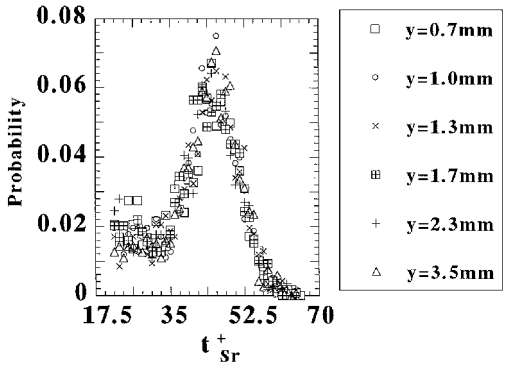

Fig. 3 Probability distributions of the Strouhal period for various y positions at $x = 70$ mm.

Table 1 Timescale and distances normal to the wall, which define the Λ shape at various streamwise locations

x, mm	x^+	y_Λ, mm	y^+_Λ	t_Λ, ms	t^+_Λ
50	875	0.9	16	4.8	21
60	1050	1.3	23	4.6	20
70	1225	1.5	26	4.8	21
80	1400	1.9	30	6.4	28
90	1575	1.9	33	4.6	20
100	1750	2.3	40	4.1	18
110	1925	2.5	44	3.9	17
120	2100	2.5	44	4.3	19

From the computed correlations the times were specified that corresponded to maximum values of the cross correlations. These times for each quadrant are schematically presented in Fig. 4 for various y positions across the boundary layer and for $x = 60$, 80, and 110 mm or $x^+ = 1050$, 1400, and 1925, respectively. The time between $t^+ = 0$ and 46 corresponds to the time between two successive von Kármán vortices of the wake with positive vorticity. Symbols corresponding to the various quadrant events are denoted in Fig. 4. This procedure was performed for the various x positions between 50 and 150 mm (x^+ between 875 and 2625), and figures similar to Fig. 4 offer important qualitative information about the sequence of events occurring across the boundary layer and how they evolve with streamwise distance during the wake-induced transition. Two time sequences of elementary coherent structures were observed along the transition region, depending on the distance from the wall. They were sequence S1—ejection, interaction wallward, interaction outward, sweep; and sequence S2—interaction wallward, ejection, interaction outward, sweep. Sequence S1 was observed close to the wall (approximately at y^+ distances between 12 and about 60), whereas sequence S2 was observed for distances farther away from the wall ($y^+ > 70$–80). Their difference was observed in the sequence of ejections and interactions wallward. The y extent in which sequence S1 occurs is a function of the streamwise distance. Within this y extent the time delay distributions between ejections and interactions wallward have a characteristic Λ shape, as schematically indicated in Fig. 4, for $x^+ = 1400$ ($x = 80$ mm). This Λ shape was detected at streamwise distances between 40 and 80 mm (x^+ between 700 and 1400, respectively). Farther downstream, the S1 sequence is still detected, whereas the Λ shape cannot be clearly distinguished. The dimensionless timescales t^+_Λ ($t^+_\Lambda = t_\Lambda u^2_\tau/\nu$, where t_Λ is the timescale) and the dimensionless y extent of the Λ shape y^+_Λ ($y^+_\Lambda = y_\Lambda u_\tau/\nu$) can be specified from diagrams similar to the ones shown in Fig. 4. These scales are presented in Table 1 for the various streamwise distances; the structures grow in y scale with streamwise distance.

C. Ensemble-Average Technique and Ensemble-Averaged Flow Structure

A further treatment of the velocity and gradient signals was applied to isolate the most representative events that occur in the wake-induced transition region. To this end, an ensemble-average technique was applied, which is described next.

As was already mentioned, the Strouhal period in the wake was identified from the signals of the gradient probe. The Strouhal periods varied in a range shown in Fig. 3; the most probable Strouhal period, however, for all x and y positions was 10.5 ms. During the ensemble-average analysis, only segments of the $\mathrm{d}U/\mathrm{d}y$ signal that corresponded to the most probable Strouhal period were considered. Simultaneous to those gradient signal segments, the u- and v-velocity signals were selected. These signals were further used to compute the instantaneous values of the quantities $uv(t)$, $u^2v(t)$,

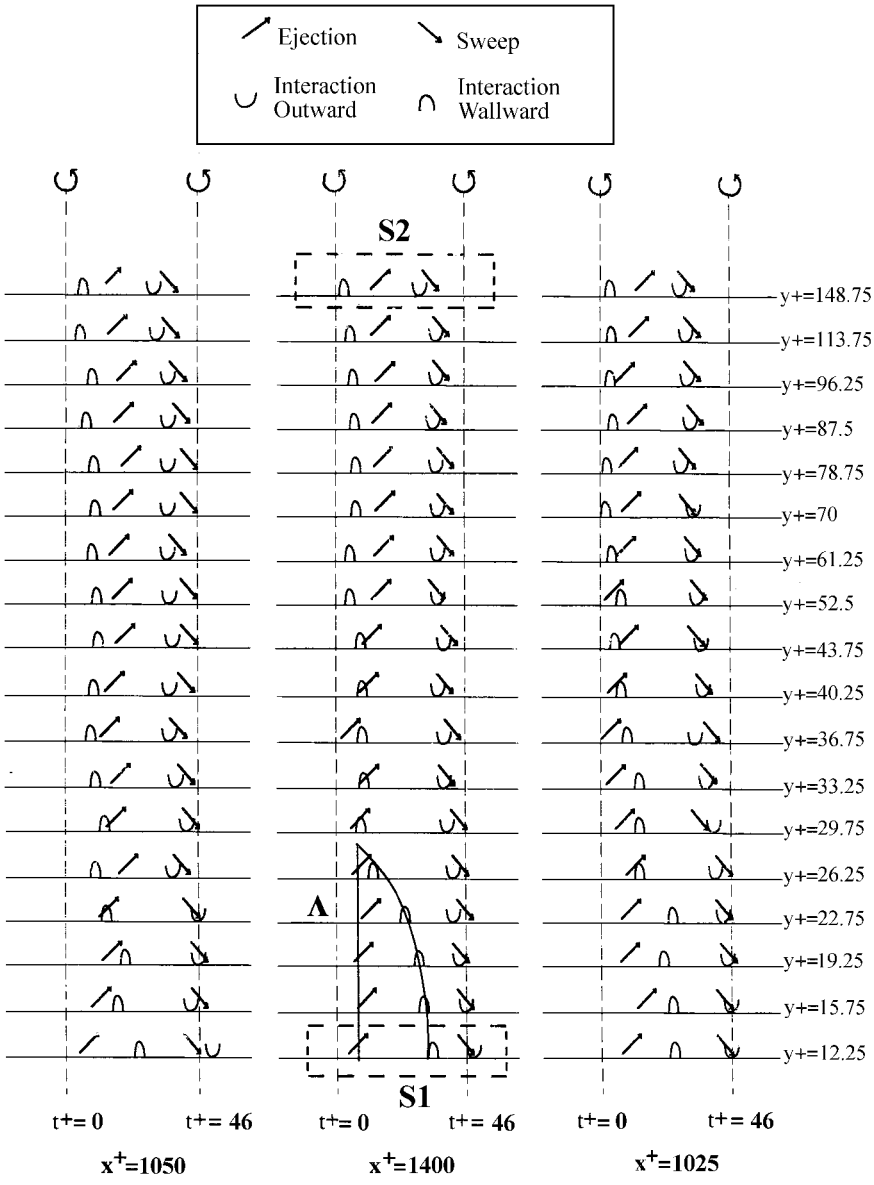

Fig. 4 Time sequence of elementary events across the boundary layer for three streamwise positions.

and $v^3(t)$. A further treatment of the signal segments was based on the level of the instantaneous uv. More specifically, values of $uv(i)$ were filtered out according to the following relation:

$$uv_{\text{mean}}(i) - \xi uv_{\text{rms}}(i) < uv(i) < uv_{\text{mean}}(i) + \xi uv_{\text{rms}}(i) \qquad (8)$$

Here, i presents a phase time in the selected Strouhal period (between $t = 0$ and 10.5 ms) $uv_{\text{mean}}(i)$ and $uv_{\text{rms}}(i)$, corresponding to ensemble averages and rms values of the uv signal and computed from the signal segments of the most probable period, respectively. The number ξ, a threshold parameter, attained the values 1 or 2, corresponding to the 68.27 or 95.45% of the uv signal sample, respectively. In this work only the ensemble averages of the quantities $uv(t)$, $u^2v(t)$, and $v^3(t)$, which correspond to the value $\xi = 1$, are reported. In this way the uv signal was filtered, excluding very high or very low uv values. From the uv satisfying relation (8), an ensemble average was computed, corresponding to the instant i, $\langle uv(i)\rangle$, according to the relation

$$\langle uv(i)\rangle = \sum_{j=1}^{n-k} uv(j, i)/(n-k) \qquad (9)$$

The number n is a counter of all of the members of the ensemble that satisfy the condition of having a Strouhal period equal to the most probable value (10.5 ms); on the other hand, k is a counter that excludes from the ensemble average those members that do not satisfy threshold condition (8). In the same way, the corresponding ensemble averages of the quantities $\langle u^2v(i)\rangle$ and $\langle v^3(i)\rangle$ were computed, and they are presented in the next paragraph.

The purpose of the just-described ensemble-average technique was the identification of the most characteristic structures that occurred during the strong wake-induced transition along the flat plate. To this end, from the ensemble-averaged velocity component $\langle u(i, y)\rangle$ the stream function $\Psi(i, y)$ was computed from the relation $\langle u\rangle(i, y) = \partial\Psi(i, y)/\partial y$. To every instant i there is a corresponding streamwise distance x_i according to a relation of the form $x_i = U_c i$ (where U_c is a local convection velocity). For every instant i between zero and 10.5 ms, the values of the stream function $\Psi(i, y_m)$ at various y positions y_m were determined from the relation

$$\Psi(i, y_m) = \Psi(i, y_{m-1}) + \langle u\rangle(i, y_m)\,\mathrm{d}y \qquad (10)$$

Here, $\mathrm{d}y$ is the increment in the y direction, the number of which was determined by the number of y locations, where measurements were conducted. Data covered y distances near the wall (between $y = 0.7$ and 3.5 mm). The number of these measurements for every x position was about 30, whereas the number of i instants at which the computation of the stream function was carried out was about 40, specified by the data sampling frequency. In this manner the computed stream function contours gave a picture of the flow structure

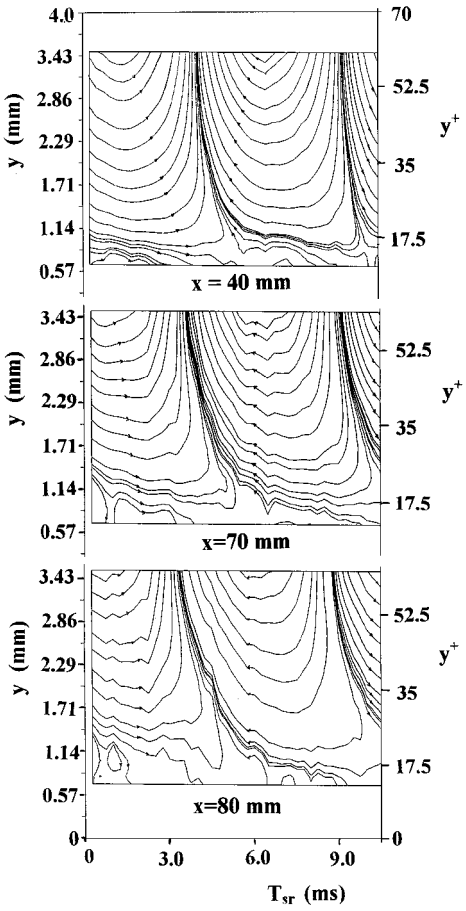

Fig. 5 Ensemble-averaged flow pattern during a Strouhal period for three streamwise positions.

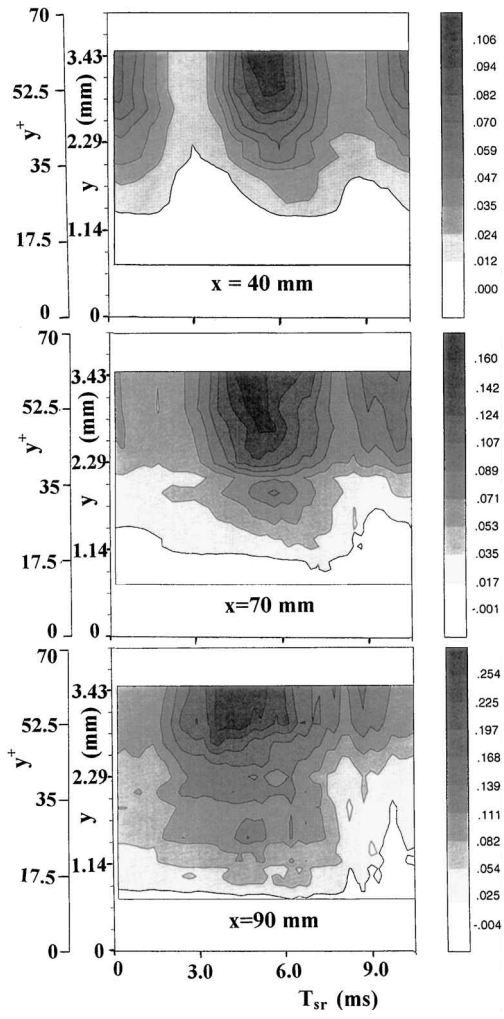

Fig. 6 Contours of the ensemble-averaged Reynolds stress for three streamwise positions.

near the wall. In Fig. 5 the ensemble-averaged contours of the stream function Ψ are shown for the streamwise locations $x = 40$, 70, and 80 mm (or $x^+ = 700$, 1225, and 1400, respectively) of the transition region. For streamwise distances smaller than $x^+ = 578$ (transition onset), the wall flow was laminar, whereas away from the wall the features of the von Kármán vortices were depicted in the stream function contours. In Fig. 5 the ensemble-averaged contours of the stream function $\Psi(i, y)$ at $x = 40$ mm ($x^+ = 700$), close to the transition onset ($x = 33$ mm), are shown. The ensemble-averaged flow pattern of the von Kármán structure can be observed at distances from the wall greater than $y^+ = 20$, whereas a vortex with negative vorticity appears initially, followed by the von Kármán vortex of positive vorticity. In Fig. 5 the time T_{sr} and the streamwise distance x increase in opposite directions. In Fig. 5 at the streamwise position $x = 70$ mm ($x^+ = 1225$), a secondary vortical structure with positive vorticity appears in the wall region. This structure occurs simultaneously with the passage of the von Kármán vortex with negative vorticity. On the other hand, during the passage of the von Kármán vortex of positive vorticity no important activity in the wall region is observed. For all x positions the secondary structure occurs simultaneously with the passage of the von Kármán vortex with negative vorticity. The timescale of the induced secondary structure decreases with the streamwise distance, whereas its length scale in the y direction increases with streamwise distance. Figure 5 shows that, for $x = 80$ mm ($x^+ = 1400$), the secondary structure has been convected to higher distances from the wall. These phenomena can also be observed at the distance $x = 90$ mm ($x^+ = 1575$); they disappear at the streamwise position $x^+ = 1750$ ($x = 100$ mm). Typical length scales of the secondary structure, which were estimated from the plots similar to Fig. 5, are around 20 wall units in the y direction and 150 wall units in the streamwise direction. From similar contour diagrams as in Fig. 5, the secondary structure reappeared at around $x^+ = 1925$.

At $x^+ = 2100$ the organized von Kármán structure could still be detected, whereas for greater streamwise distances the vortex with positive vorticity approached the wall and the secondary structure could not be detected any more. For distances greater than $x = 170$ mm ($x^+ = 2975$), no Strouhal frequency could be identified in the velocity spectra; consequently the ensemble-average analysis could not be applied.

D. Ensemble-Averaged Contours of $\langle uv \rangle$, $\langle u^2 v \rangle$, and $\langle v^3 \rangle$

The ensemble-average technique described in the preceding paragraph was applied to the Reynolds stress signal uv and to the signals of turbulent kinetic energy transfer terms $u^2 v$ and v^3. This computation was focused on the region near the wall (up to $y = 3.5$ mm) and for streamwise distances between 40 and 150 mm ($x^+ = 700$ to 2825). Contours of the ensemble-averaged values of these terms were computed during the most probable Strouhal period. Figure 6 shows the Reynolds-stress ensemble-averaged contours for three streamwise positions $x = 40$, 70, and 90 mm ($x^+ = 700$, 1225, and 1575). The $\langle uv(i) \rangle$ values near the wall at the streamwise position $x = 40$ mm are low and positive. Farther downstream, the $\langle uv(i) \rangle$ values are also low and sometimes negative. Nevertheless, these low values are within the experimental error. The contours in Fig. 6 at greater y distances correspond to higher $\langle uv(i) \rangle$ values and show clearly the influence of the von Kármán vortices, taking an ellipsoidal shape. Figures 7 and 8 show the contours corresponding to the transfer terms $\langle u^2 v(i) \rangle$ and $\langle v^3(i) \rangle$ for the same streamwise distances as in Fig. 6. Both transfer terms change signs during the passage of the external wake vortices of positive or negative vorticity. Negative values of both transfer terms correspond to the passage of the wake vortex with negative vorticity. According to the contours of the transfer terms, it is proposed that, during the passage of the negative vorticity wake vortices, turbulent kinetic energy of the u and v velocity components is transferred from the outer flow region

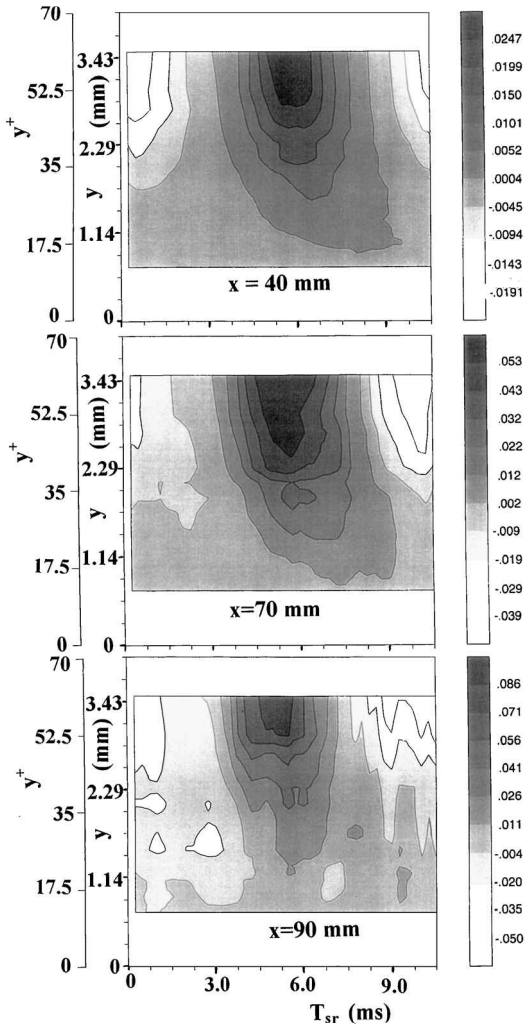

Fig. 7 Contours of the ensemble-averaged transfer term $\langle u^2 v \rangle$ for three streamwise positions.

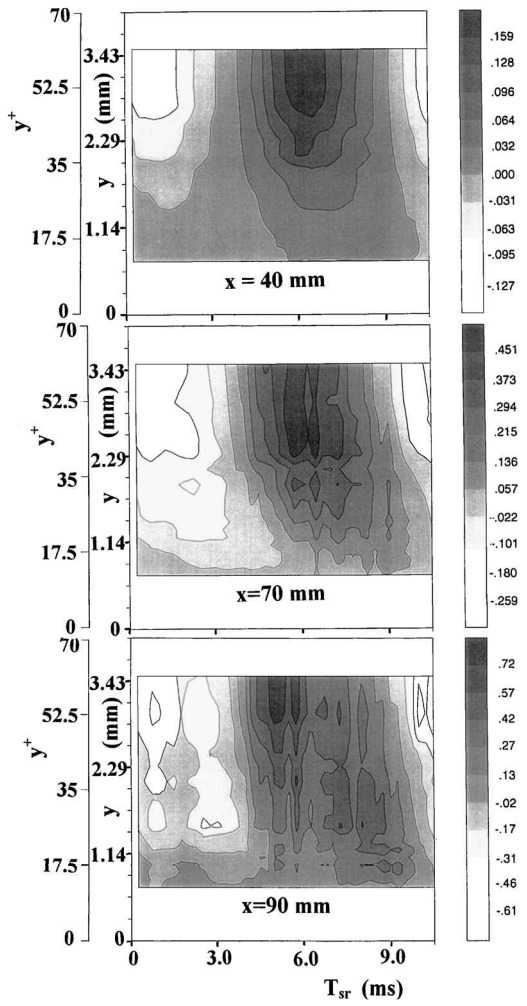

Fig. 8 Contours of the ensemble-averaged transfer term $\langle v^3 \rangle$ for three streamwise positions.

(wake) toward the wall. Similarly, during the passage of the von Kármán vortex of positive vorticity, when the transfer terms obtain their maximum positive values, turbulent kinetic energy of the u and v velocity components is transferred from the wall toward the outer region.

IV. Discussion

In Fig. 9 two ideal vortices having opposite signs of vorticity are schematically shown together with the time sequences S1 and S2 of the elementary coherent structures that occur during the passage of the von Kármán vortices. In the same figure the elementary structures that are associated with the vortices of positive and negative signs are presented. Sequence S2, which was observed at distances away from the wall, could be associated with the passage of the von Kármán structure. For sequence S1, which was observed close to the wall, one could suggest that the Λ shape corresponds qualitatively to the secondary structure; this is shown in Fig. 5 by observing the stream functions. The sequence of an ejection, followed by an interaction wallward, occurs simultaneously with the passage of the vortex with negative vorticity of the von Kármán structure in the outer region. The streamlines in Fig. 5 show clearly the occurrence of the secondary structure simultaneously with the passage of the von Kármán vortex with vorticity of opposite sign. In the same way, the upper part of the secondary structure corresponds qualitatively to the instantaneous passage of an ejection followed by an interaction wallward. The data suggest that the passage of each vortex pair induces a single sequence of events close to the wall. The streamwise position and the timescales of the secondary structure are in agreement with the ones of the Λ shape, up to the streamwise distance of $x^+ = 1400$.

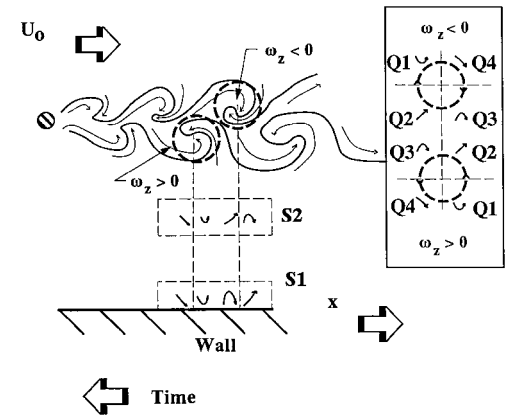

Fig. 9 Sketch of two wake vortices and event sequences S1 and S2.

Farther downstream, the secondary structure is convected to higher distances from the wall, where the Λ shape gradually disappears.

The distribution of the intermittency factor in the streamwise direction, presented in Fig. 2, shows a deviation from the distribution predicted by relation (1), especially in the streamwise region between $x = 70$ and 110 mm. In the same streamwise region the secondary structure, identified from the contours of the stream function (Fig. 5), is developed while remaining in the region near the wall. Around $x = 90$ mm, where a local maximum in the γ distribution occurs, the secondary structure is still in the near-wall region, while its scale reaches its maximum value. In the streamwise region between 90 and 110 mm, the secondary structure is lifted away

from the wall; therefore, a decrease in the intermittency factor is expected because γ is measured at $y = 0.7$ mm ($y^+ = 12$). At $x =$ 110 mm, a reappearance of the secondary structure takes place near the wall; hence, the intermittency factor starts increasing again with x, approaching unity farther downstream where the transitional flow tends to become a fully developed turbulent flow.

Doligalski and Walker[1] and Peridier et al.[24] studied numerically the receptivity of a boundary layer disturbed by a vortex structure of negative vorticity moving in a uniform velocity field. Using several convection velocities of the structure and preserving its distance from the wall constant, their computations showed that for a critical convection velocity a lift-up of the boundary-layer streamlines occurred. This phenomenon was associated with a local increase in the boundary-layer thickness. The flow is separated during the passage of the (ideal) vortex structure, developing a secondary vortical structure near the wall. This vortical structure was of the same positive vorticity as the secondary vortex identified in the present work, whereas no separation of the boundary-layer flow could be detected here in a fixed frame. This is a qualitative comparison between the two investigations because the von Kármán vortex street is far more complicated than the idealized vortex considered by Doligalski and Walker.[1]

On the basis of conditional analysis of their experimental data, Rajagopalan and Antonia[25] suggested that in the wall region of a turbulent boundary layer transverse vortices could be associated to others of opposite vorticity. The present work verifies this fact only for the negative transverse vortex. During the passage of the vortex with positive vorticity of the von Kármán structure, no negative vorticity structure was detected near the wall.

Klewick et al.[26] studied the correlation between transverse vortices and the turbulent kinetic energy transfer mechanism in the wall region of turbulent boundary layers. They measured a positive $v\omega_z$ value associated with a change in turbulent kinetic energy production. The positive $v\omega_z$ term indicates that a negative vorticity structure can be combined with negative v fluctuations of the velocity. This fact is also confirmed by the present measured values of $\langle v^3 \rangle$ and $\langle u^2 v \rangle$ in the wall region.

Luton et al.[6] simulated numerically the interaction of a spanwise vortex with a flat-plate boundary layer. They concluded that a sufficiently strong negative vortex induces an eruption of opposite sense vorticity and the generation of a secondary vortex. The secondary vortex induced an upward motion of the primary vortex. This response of the primary vortex, called the *rebound phenomenon*, has been observed also by other investigators (e.g., Refs. 27 and 28). In the present work the rebound phenomenon could not be identified. The development and lift up of the secondary structure with positive vorticity, however, indicate a possible rebound of the von Kármán vortex with negative vorticity.

The present work can be considered as having a broader significance. During the interaction of the cylinder wake with the boundary layer, the flow phenomena can also be understood as a traveling wave, which the plate senses in the form of a wavy disturbance convected downstream. A way to gain better insight into these phenomena would be to determine the pressure distribution along the plate.

V. Conclusions

Structural aspects of a strong wake-induced transition on a flat plate have been experimentally investigated. Combining the quadrant-splitting analysis of the streamwise and normal-to-the-wall velocity signals and the cross correlation between velocity and gradient signals, a mean picture of the flow with respect to the four elementary motions (quadrants) has been inferred. Away from the wall, the time sequence of the quadrants (interaction wallward–ejection–interaction outward–sweep) is the result of the induced flow by the von Kármán street. In the region near the wall ($y^+ < 60$), the time sequence is altered (ejection–interaction wallward–interaction outward–sweep). Applying a combined ensemble-average and filtering technique, a picture of the most characteristic flow elements can be inferred. The conclusion is made that during the strong wake-induced transition a secondary structure is formed near the wall simultaneously with the passage of the vortex with negative vorticity. The secondary vortical structure possesses positive vorticity and starts forming at the transition onset; it grows initially in scale and at a streamwise location of about 110 mm is lifted up. A reappearance of the secondary structure is observed farther downstream at approximately 120 mm. The conclusion is also made that during the passage of the negative vorticity wake vortices turbulent kinetic energy of the u and v velocity components is transferred from the outer flow region (wake) toward the wall, whereas during the passage of the wake vortex with positive vorticity turbulent kinetic energy of the u and v velocity components is transferred from the wall toward the outer region.

Acknowledgments

This work has been supported by BRITE/EURAM Area 3, Contract AERO-CT92-0050. The authors are indebted to one of the reviewers for the comments included in the last paragraph of the discussion section.

References

[1] Doligalski, T. L., and Walker, J. D. A., "The Boundary Layer Induced by a Convected Two-Dimensional Vortex," *Journal of Fluid Mechanics*, Vol. 139, Feb. 1984, pp. 1–28.

[2] Walker, J., "Wall Layer Eruptions in Turbulent Flows," *IUTAM Symposium on Structure of Turbulence and Drag Reduction*, edited by A. Gyr, Springer–Verlag, Zurich, 1989, pp. 109–117.

[3] Ersoy, S., and Walker, J. D. A., "Viscous Flow Induced by Counter-Rotating Vortices," *Physics of Fluids*, Vol. 28, No. 9, 1985, pp. 2687–2698.

[4] Ersoy, S., and Walker, J. D. A., "The Boundary Layer Due to a Three-Dimensional Vortex Loop," *Journal of Fluid Mechanics*, Vol. 185, Dec. 1987, pp. 569–598.

[5] Gartshore, I. S., Durbin, J. C., and Hunt, J. C. R., "The Production of Turbulent Stress in a Shear Flow by Irrotational Fluctuations," *Journal of Fluid Mechanics*, Vol. 137, Dec. 1983, pp. 307–329.

[6] Luton, A., Ragab, S., and Telionis, D., "Interactions of Spanwise Vortices with a Boundary Layer," *Physics of Fluids*, Vol. 7, No. 11, 1995, pp. 2757–2765

[7] Squire, L. C., "Interactions Between Wakes and Boundary Layers," *Progress in Aerospace Sciences*, Vol. 26, No. 3, 1989, pp. 261–288.

[8] Savill, A., and Zhou, M., "Wake/Boundary Layer and Wake/Wake Interactions—Smoke Flow Visualization and Modeling," *Proceedings of the 2nd Asian Congress of Fluid Mechanics*, edited by N. M. C. Ko, Science Press, Beijing, 1983, pp. 743–754.

[9] Kyriakides, N. K., Kastrinakis, E. G., Nychas, S. G., and Goulas, A., "Prediction of Boundary Layer Transition Induced by a von Karman Vortex Street Wake," *Journal of Aerospace Engineering*, Vol. 210, No. G2, 1996, pp. 167–179.

[10] Kyriakides, N. K., Fotea, K., Kastrinakis, E. G., Goulas, A. I., and Nychas, S. G., "Boundary Layer Transition Induced by a von Karman Vortex Street Wake," *Advances in Turbulence V*, edited by R. Benzi, Kluwer Academic, Norwell, MA, 1995, pp. 281–285.

[11] Van Atta, C., and Gharib, M., "Ordered and Chaotic Vortex Streets Behind Circular Cylinders at Low Reynolds Numbers," *Journal of Fluid Mechanics*, Vol. 174, Jan. 1987, pp. 113–133.

[12] Kastrinakis, E. G., and Eckelmann, H., "Measurement of Streamwise Vorticity Fluctuations in a Turbulent Channel Flow," *Journal of Fluid Mechanics*, Vol. 137, Dec. 1983, pp. 165–186.

[13] Wills, J. A. B., "The Correction of Hot-Wire Readings for Proximity to a Solid Boundary," *Journal of Fluid Mechanics*, Vol. 12, Pt. 3, 1962, pp. 388–396.

[14] Oka, S., and Kostic, Z., "Influence of Wall Proximity on Hot-Wire Velocity Measurements," *DISA-Information*, No. 13, May 1972, pp. 29–33.

[15] Eckelmann, H., Nychas, S. G., Brodkey, R. S., and Wallace, J. M., "Vorticity and Turbulence Production in Pattern Recognized Turbulent Flow Structures," *Physics of Fluids*, Vol. 20, No. 10, 1977, pp. S225–S231.

[16] Vukoslavcevic, P., and Wallace, J. M., "Influence of Velocity Gradients on Measurements of Velocity and Streamwise Vorticity with Hot-Wire X-Array Probes," *Review of Scientific Instruments*, Vol. 52, No. 6, 1981, pp. 869–879.

[17] Schlichting, H., *Boundary Layer Theory*, 6th ed., McGraw–Hill, New York, 1968, pp. 691–695.

[18] Cimbala, J. M., Nagib, H. M., and Roshko, A., "Large Structure in the Far Wakes of Two Dimensional Bluff Bodies," *Journal of Fluid Mechanics*, Vol. 190, May 1988, pp. 265–298.

[19] Keller, F. J., and Wang, T., "Effects of Criterion Functions on Intermittency in Heated Transitional Boundary Layers with and Without Streamwise Acceleration," American Society of Mechanical Engineers, Paper 93-GT-67, 1993.

[20] Antonia, M., "Conditionally Sampled Measurements Near the Outer Edge of a Turbulent Boundary Layer," *Journal of Fluid Mechanics*, Vol. 56, Pt. 1, 1972, pp. 1–18.

[21] Muck, K. C., "Comparison of Various Schemes for the Generation of the Turbulent Intermittency Function," Dept. of Aeronautics, Imperial College of Science and Technology, Univ. of London, Rept. 80-03, London, March 1980.

[22] Dhawan, S., and Narasimha, R., "Some Properties of Boundary Layer Flow During Transition from Laminar to Turbulent Motion," *Journal of Fluid Mechanics*, Vol. 3, Pt. 4, 1958, pp. 418–436.

[23] Wallace, J., Eckelmann, H., and Brodkey, R., "The Wall Region in Turbulent Shear Flow," *Journal of Fluid Mechanics*, Vol. 54, Jan. 1972, pp. 39–48.

[24] Peridier, V. J., Smith, F. T., and Walker, J. D., "Vortex-Induced Boundary Layer Separation," *Journal of Fluid Mechanics*, Vol. 232, Pts. 1 and 2, Nov. 1991, pp. 99–133.

[25] Rajagopalan, S., and Antonia, R., "Structure of the Velocity Field Associated with the Spanwise Vorticity in the Wall Region of a Turbulent Boundary Layer," *Physics of Fluids*, Vol. 5, No. 10, 1993, pp. 2502–2510.

[26] Klewick, J. C., Murray, J. A., and Falco, R. E., "Vortical Motion Contributions to Stress Transport in Turbulent Boundary Layers," *Physics of Fluids*, Vol. 6, No. 1, 1994, pp. 277–286.

[27] Harvey, J. K., and Perry, F. J., "Flowfield Produced by Trailing Vortices in the Vicinity of the Ground," *AIAA Journal*, Vol. 9, No. 8, 1971, pp. 1659, 1660.

[28] Peace, A. J., and Riley, N., "A Viscous Vortex Pair in Ground Effect," *Journal of Fluid Mechanics*, Vol. 129, April 1983, pp. 409–426.

J. P. Gore
Associate Editor